Structural Engineering and Mechanics, *Vol. 68, No. 4 (2018) 475-483*
DOI: https://doi.org/10.12989/sem.2018.68.4.475

Behavior of improved through-diaphragm connection to square tubular column under tensile loading

Ying Qin*[1,2], Jing-Chen Zhang[1], Peng Shi[1], Yi-Fu Chen[1], Yao-Han Xu[1] and Zuo-Zheng Shi[1]

[1]*Key Laboratory of Concrete and Prestressed Concrete Structures of Ministry of Education, and National Prestress Engineering Research Center, School of Civil Engineering, Southeast University, Nanjing, China*
[2]*State Key Laboratory of Subtropical Building Science, South China University of Technology, Guangzhou, China*

(Received April 16, 2018, Revised October 5, 2018, Accepted October 11, 2018)

Abstract. Square tubular columns are commonly used in moment resisting frames, while through-diaphragm connection is the most typical configuration detail to connect the H-shaped beam to the column. However, brittle fracture normally occurs at the complete joint penetration weld between the beam flange and the through-diaphragm due to the stress concentration caused by the geometrical discontinuity. Accordingly, three improved types of through-diaphragm are presented in this paper to provide smooth force flow path comparing to that of conventional connections. Tensile tests were conducted on four specimens and the results were analyzed in terms of failure modes, load-displacement response, yield and ultimate capacity, and initial stiffness. Furthermore, strain distributions on the through-diaphragm, the beam flange plate, and the column face were comprehensively evaluated and discussed. It was found that all the proposed three types of improved through-diaphragm connections were able to reduce the stress concentration in the welds between the beam flange and the through-diaphragm. Furthermore, the stress distribution in connection with longer tapered through-diaphragm was more uniform.

Keywords: strain analysis; tensile performance; through-diaphragm; square tube column; load-displacement curve

1. Introduction

Square tubular column has been increasingly attractive in engineering design in areas of high seismic risk. More than 80% of steel multi-story moment frames in China and Japan utilize square tubular column due to its structural and aesthetic merits (Shahraki *et al.* 2018). Square tubular column exhibits excellent bending resistance around the main axis as most of the materials are efficiently made use of and arranged far from the neutral axis. Meanwhile, it has larger torsional capacity over conventional open section column because of closed shape and thus, reduces the need to laterally support the column and alleviate the strength deterioration caused by column rotation (Nunez *et al.* 2017, Zhang *et al.* 2018).

Despite the awareness of the advantages mentioned above, square tubular column has some limitations comparing to wide flange sections. For instance, it is difficult to have access to the internal space of the column for bolting or welding. It is also difficult to do welding inspection and therefore, the production cost grows (Shahidi *et al.* 2015, Qin *et al.* 2016). Consequently, extensive research has been conducted to propose appropriate details for reducing the cost while maintaining proper seismic performance.

Kim *et al.* (2008) and Nia *et al.* (2013) evaluated the seismic response of pre-Northridge fully restrained steel moment connections between H-shaped beams and square tubular columns. It was found that the connections are likely to fail in a brittle manner caused by the crack of the beam flange complete joint penetration (CJP) welds. Goswami and Murty (2010) suggested to use inclined rib plates to ensure planar continuity between H-shaped beam and square tubular column webs. Numerical simulations indicated that the proposed connection behaved better than conventional connections. Torabian *et al.* (2012) presented detailed analysis and design procedure for a diagonal through-plate connection with built-up box column. Nia *et al.* (2014) experimentally investigated the connections composed of square tubular column and steel beam reinforced by finger-shaped flange plate. The suitable arrangement of both the transverse and the longitudinal fillet weld in the top flange plate was suggested. Wang and Wang (2016) studied the yield and ultimate capacities of the blind bolted endplate to square tubular column connection in joint tensile region. Mirghaderi *et al.* (2010) proposed an innovative fabrication-easy connection between steel beam and tubular column. The connection was composed of a vertical plate passing through the column and welded to the column flanges. The beam was then connected to the through plate. The test results indicated that the connection was capable of absorbing energy before experiencing strength deterioration. Qin *et al.* (2015a, b) used component-based model to behavior of through-diaphragm connection to concrete-filled tubular column with H-beam or beam flange under tension. Recently, Hadianfard *et al.* (2017) established a numerical model for X-braced frame and the influences of different connection configurations on structural behavior have been evaluated. Rezaifar *et al.*

*Corresponding author,
E-mail: qinying@seu.edu.cn

ISSN: 1225-4568 (Print), 1598-6217 (Online)

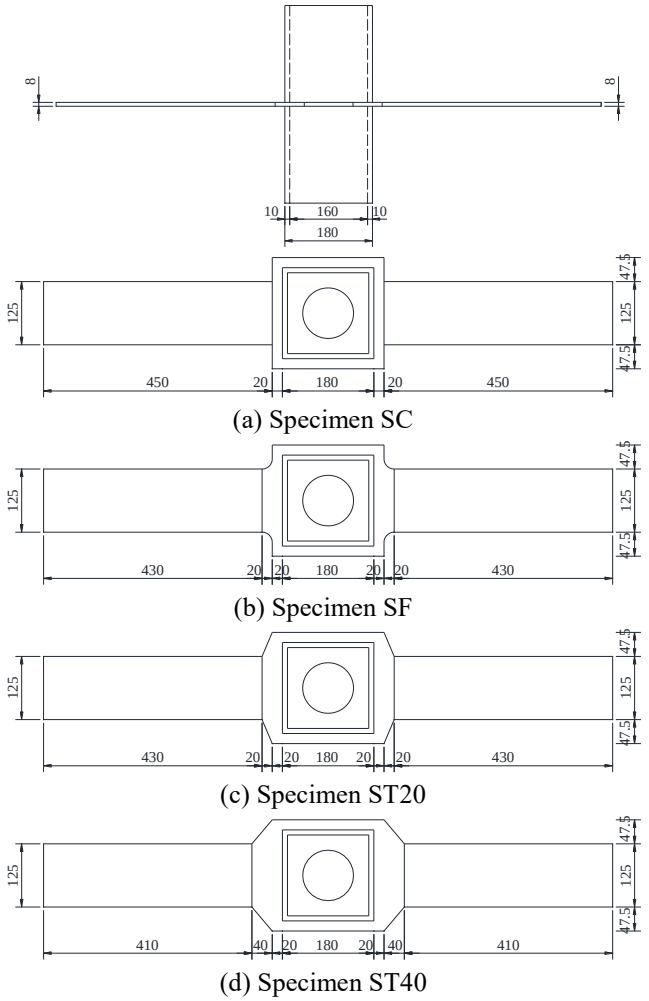

(a) Specimen SC

(b) Specimen SF

(c) Specimen ST20

(d) Specimen ST40

Fig. 1 Specimen details

(2017) experimentally investigated the structural behavior of interior-diaphragm and exterior-diaphragm connections. Rong *et al.* (2018) conducted tensile tests on four square hollow section column connections with exterior diaphragms. An analytical model was proposed to predict the bearing capacity of this connection. Zohra *et al.* (2018) used ANSYS to carry out the numerical simulation of semi-rigid connections and an approach was proposed to define a more accurate evaluation about semi-rigid connections. De Nardin *et al.* (2018) carried out tests on through-bolted connections subjected to pure shear loading. The tests showed that the contribution of the mechanical shear connectors is not significant when the connection is included in the push out tests. De Domenico *et al.* (2018) investigated the static structural response of steel frames with partially restrained connections through a probabilistic framework. Wang *et al.* (2018) proposed a design procedure for bolted frames with semi-rigid connections. Dehghan *et al.* (2018) evaluated the seismic behavior of built-up double-I column connection with exterior diaphragm. A general review on the connections to square tubular columns can be found in Qin and Chen (2016).

The square tubular column has two parallel webs at the sides. This is different from the wide flange column which has one web at the center. The absence of web at the center may induce an increase of the column flange deformation when the flexural moment is transferred from the beam flanges to the column. Due to the out-of-plane deformation of the column flange (Qin *et al.* 2017) and the inevitable geometrical discontinuity between the beam flange and the through-diaphragm, the square tubular column experiences different performance comparing with the conventional wide flange column. Furthermore, the actual force transfer mechanism completely differs from the normally assumed pattern in connection with open-section column (Kim and Oh 2007).

The most typical configuration details of beam-to-column connections applied in Asian countries has diaphragms inside, outside, or passing through the tube column, namely interior-diaphragm, exterior-diaphragm, or through-diaphragm connections. For the through-diaphragm connections, the diaphragm penetrates the column face and extends certain distance before it is connected to beam flange by CJP groove welds, as shown in Fig. 1(a). Although this detail looks to be relatively convenient and simple, the Kobe earthquake revealed that unless improvement or reinforcement had been made in connection details, brittle fracture normally occurred at the location between the beam flange and the through-diaphragm (Kurobane 2002). One of the reasons for brittle fracture is overstress in the beam flange and beam flange CJP groove welds, owning to the abrupt geometrical change of the connection. The occurrence of these cracks reduces the rotation ability of plastic hinges at the beam ends.

This paper proposes three improved connection details to ensure smooth flow of forces from the beam to the square tubular column. Efficiency of the presented through-diaphragm configurations to transfer tensile load is proved through results of tensile tests.

2. Experimentation

2.1 Test specimen

Four specimens were designed to simulate an exterior cruciform joint subassembly. Each assembly was composed of a column and two beam flange plates. Through-diaphragm was used to connect the beam flange to the column. All specimens were constructed with a square tubular column 180×180×10×10 (mm) and two beam flange plate with the cross section of 125×8 (mm). The thickness of the through-diaphragm is 8 mm, and the height of the column is 400 mm. Fig. 1 shows these four test specimens.

Specimen SC was designed based on the conventional configuration detail of the through-diaphragm connection. ‘C’ stands for the conventional connection type. No reinforcement or improvement was made in order to investigate the load flow path for the widely-applied connection type. Fig. 1(a) presents the connection detail of Specimen SC, using the conventional connection detail for through-diaphragm.

As will be found in the discussion later, Specimen SC experienced significant stress concentration between the beam flange and the through-diaphragm. Therefore, an attempt was made to enhance the connection performance

Table 1 Material property

Type	t	f_y	f_u	f_y / f_u	*Elo.*	E_s
	mm	N/mm^2	N/mm^2		%	N/mm^2
Square tubular column	10	294	454	0.65	31	2.08×10^5
Diaphragm/beam flange plate	8	319	463	0.69	32	2.08×10^5

(a) Full view

(b) Top side

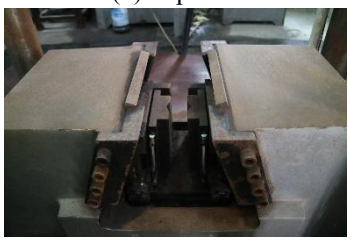

(c) Bottom side

Fig. 2 Buckling shapes with different ω values

by improve the geometry of the through-diaphragm. Fillet with a diameter of 20 mm was used in Specimen SF to alleviate the abrupt geometrical discontinuity between the beam flange and the through-diaphragm, as shown in Figure 1(b). 'F' represents the through-diaphragm is modified by fillet.

Specimens ST20 and ST40 adopted tapered through-diaphragm to connect the beam flange to the column face. 'T' stands for the tapered shape for the diaphragm. This improvement is believed to help transfer the tensile load gradually from the beam flange to the square tubular column. The difference between Specimens ST20 and ST40 was the extended length of the through-diaphragm, as illustrated in Figs. 1(c)-(d).

The mechanical properties for the square tubular column, the through-diaphragm, and the beam flange plate obtained from tensile coupon tests are given in Table 1.

2.2 Test procedure

The test was conducted under monotonic tensile loading using a MTS machine with loading capacity of 2000 kN, as illustrated in Fig. 2. The applied load and the corresponding displacement at the beam flange end were recorded automatically by the machine and recorded simultaneously by a computer. The column face, through-diaphragm, and beam flange plate were instrumented with electric-resistance strain gauges to evaluate the stress flow path and stress concentration.

The tensile load was applied in a displacement-controlled manner. The loading rate was 6.0×10^{-3} mm/s when the specimen was in the elastic range. This rate was grown up to 1.2×10^{-2} mm/s as soon as the specimen exhibited nonlinear performance, which was decided by the turning point of the load-displacement curves.

3. Test results

3.1 Global behavior and failure mode

The behavior and the failure modes of specimens varied with the design details of the connections. Their tensile performance and failure modes are briefly described below.
Specimen SC behaved in an elastic manner before the tensile load reached 311 kN. The whitewash started flaking from the beam flange plate as the load continued to increase. Specimen SC failed in a brittle mode during the loading level of 439 kN with a rapid drop in specimen capacity induced by the fracturing of the location between the through-diaphragm and the beam flange plate. The cracks initiated at the root of the complete joint penetration weld and quickly progressed through the width of the beam flange, as can be seen in Fig. 3(a).

The yielding mode of Specimen SF was quite similar to that of Specimen SC. No apparent deformation or other crack were observed during the loading procedure. The specimen began to yield when the tensile load arrived at 351 kN, as can be evident from the turning point of the load-displacement curve. Small crack was observed at the complete joint penetration weld between the through-diaphragm and the beam flange plate at the loading level of 464 kN. Once the crack occurred, the structural behavior of the specimen rapidly deteriorated. The test was terminated as the crack propagated along the width of the through-diaphragm and led to the fracture, as shown in Fig. 3(b).

For Specimen ST20, the trend of load versus displacement curve was the same as that of Specimen SF before the tensile load reached 351 kN. There was no physical deformation during the test. When the load reached 350 kN, a distinctive sound was emitted from the specimen. The ensuing abrupt fracture progressed through the width of

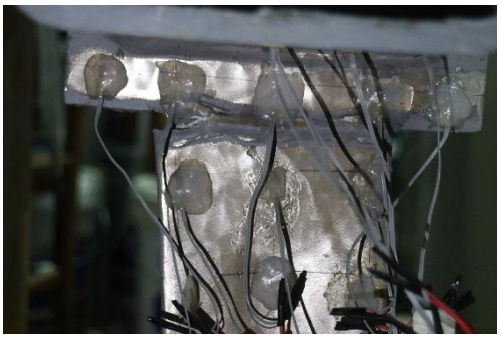

(a) Specimen SC

(b) Specimen SF

(c) Specimen ST20

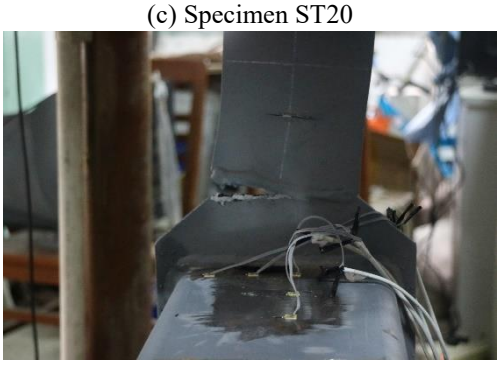

(d) Specimen ST40

Fig. 3 Failure of the tested specimens

the beam flange as shown in Fig. 3(c).

Specimen ST40 exhibited stable behavior at an early stage. Slight falling off of whitewash was found at the loading level of 330 kN. As the tensile load arrived at 380 kN, slight necking of beam flange plate was observed. Similar to Specimen ST20, the primary cause of the failure of Specimen ST40 was the crack between the through-diaphragm and the beam flange plate corresponding to the loading of 398 kN. Simultaneously, another crack was observed in the flange plate at a distance about 110 mm from the column face, as shown in Fig. 3(d).

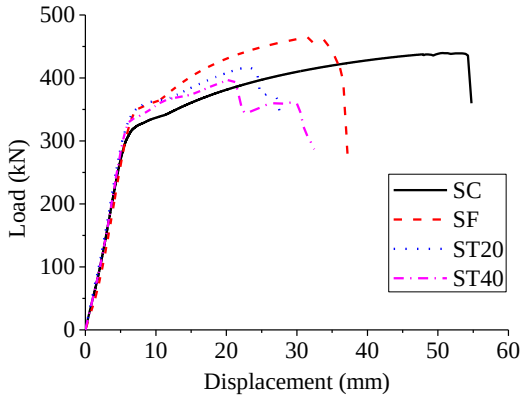

Fig. 4 Load versus displacement response

Table 2 Test results

Specimen	δ_y	F_y	δ_u	F_u	K_E	μ
	mm	kN	mm	kN	kN/mm	
SC	6.24	311.27	50.67	439.52	60.24	8.12
SF	7.49	351.03	31.51	464.70	61.34	4.21
ST20	7.26	351.05	23.45	416.08	62.94	3.23
ST40	6.17	330.08	20.85	398.17	62.54	3.38

3.2 Load versus displacement response

Fig. 4 shows the load versus displacement curves for four specimens. The test value obtained for yield tensile load F_y and the corresponding displacement δ_y, the ultimate tensile load F_u and the corresponding displacement δ_u, the initial stiffness K_E, and the ductility ratio μ are summarized in Table 2. The ductility ratio is defined as the ratio of the displacement corresponding to the ultimate capacity to yield one.

It can be seen that the responses of all specimens are similar before the yielding occurs. The displacement gradually increases as the loading level continues to grow. A sudden drop in load-bearing capacity at the end of the test is caused by the fracture of the specimens.

From the theoretical point of view, the yield and ultimate tensile loads for different specimens should be the same, since all specimens, except for Specimen SF, are failed by the fracture of the beam flange plate. It means the capacity of the specimens is dominated by the capacity of the beam flange plate. This is expected as all the specimens are designed according to the strong-column-weak-beam criterion. Slight differences of load capacities among four specimens shown in Table 2 are believed to be caused by the deviation of material property of steel. Furthermore, four specimens with different types of through-diaphragms can provide almost the same initial stiffness. This can be explained by the fact that the deformation of the specimens is largely contributed from that of the beam flange and the square tubular column, while the differences caused by the through-diaphragm can be ignored.

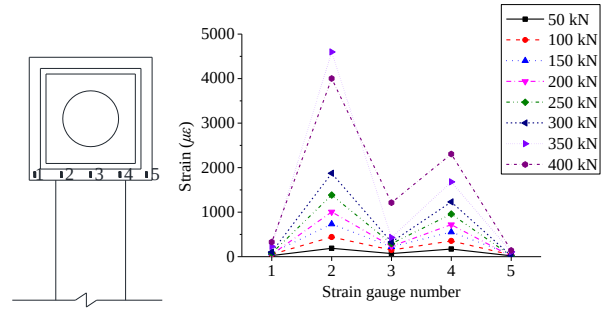

(a) Specimen SC

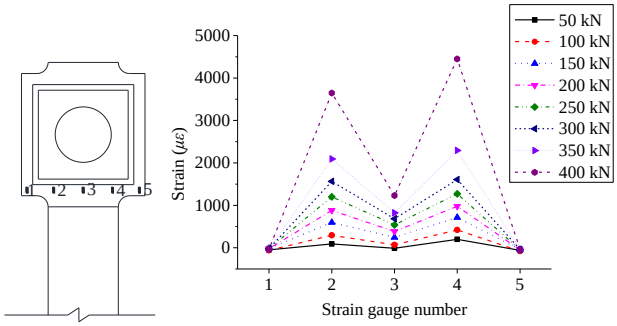

(b) Specimen SF

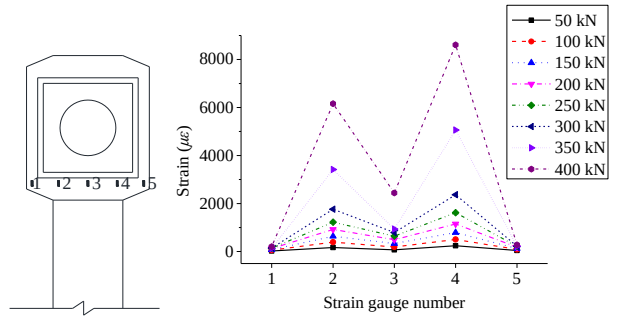

(c) Specimen ST20

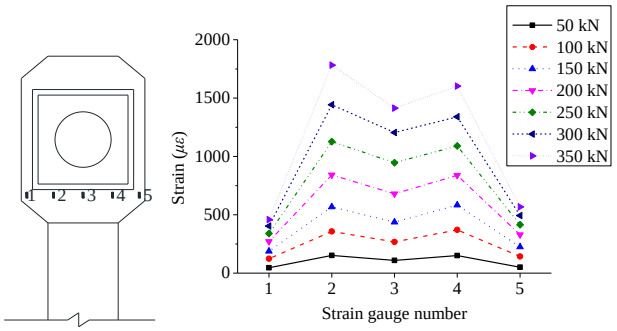

(d) Specimen ST40

Fig. 5 Strain analysis on gauges 1-5

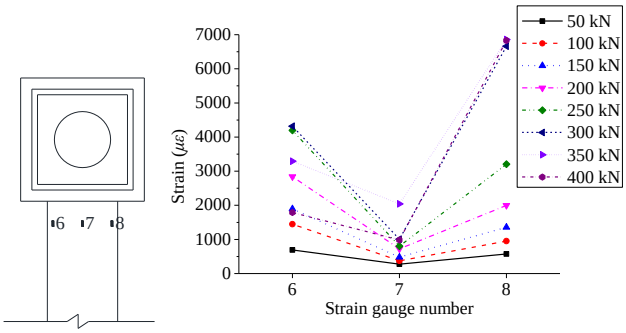

(a) Specimen SC

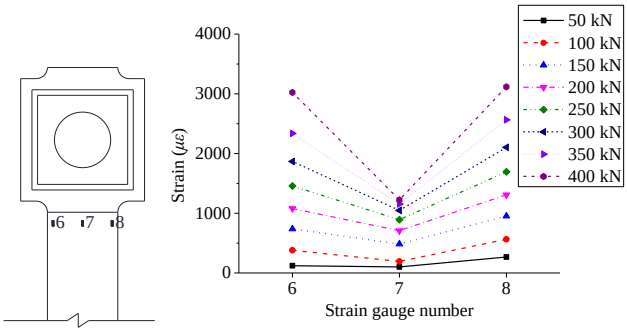

(b) Specimen SF

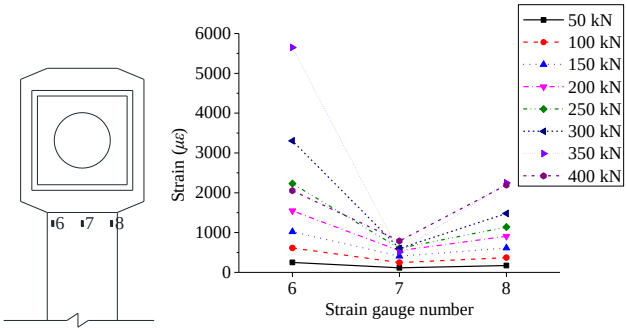

(c) Specimen ST20

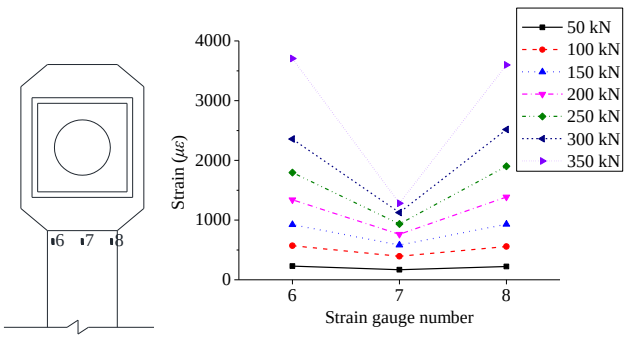

(d) Specimen ST40

Fig. 6 Strain analysis on gauges 6-8

3.3 Strain analysis by load-step

Strain analysis was conducted between the conventional through-diaphragm connection type and the improved through-diaphragm type, using the values recorded by the strain gauges arranged on the column flange, the beam flange plate, and the through-diaphragm of Specimens SC, SF, ST20, and ST40. It should be noted that a few of the mounted strain gauges were out of work during the test, and the data from these strain gauges were excluded in the analysis.

Strain distribution of the through-diaphragm at the location close to column face is illustrated at each load-step in Fig. 5. The yielding strains for the column and the beam flange/through-diaphragm are 1413 $\mu\varepsilon$ and 1534 $\mu\varepsilon$, respectively. is It can be observed that for conventional through-diaphragm connection type, most of the tensile force is transferred to the sides of the column. This means considerable amount of tensile force is finally carried by the web of the square tubular column. It is also clear that the

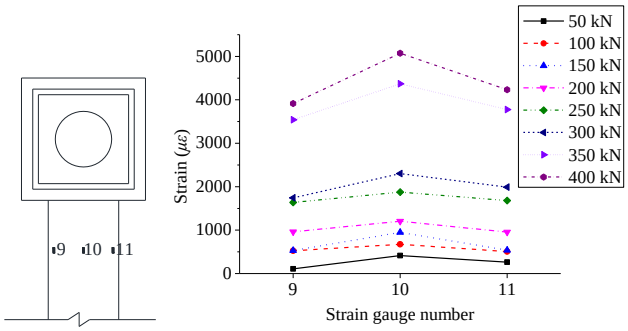

(a) Specimen SC

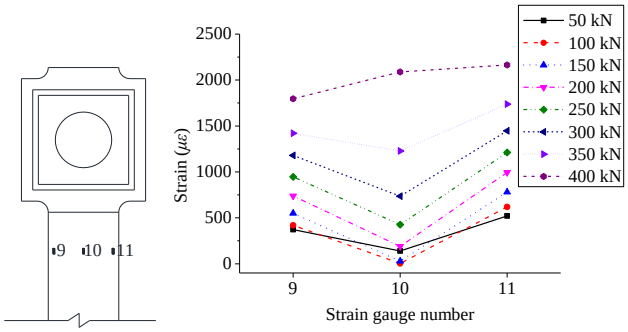

(b) Specimen SF

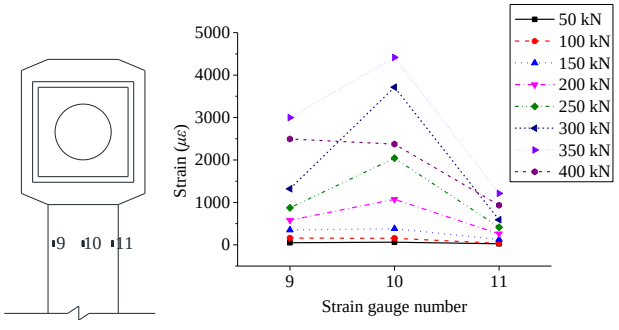

(c) Specimen ST20

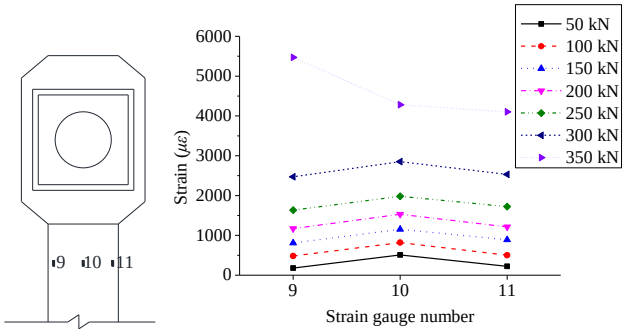

(d) Specimen ST40

Fig. 7 Strain analysis on gauges 9-11

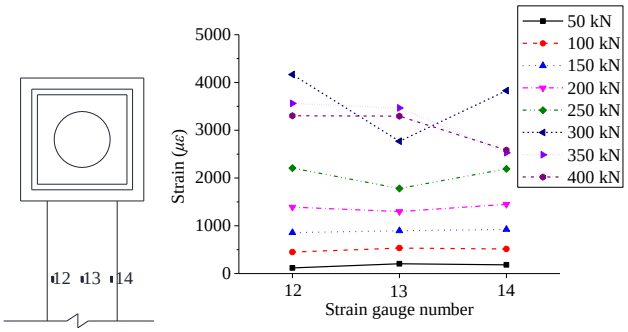

(a) Specimen SC

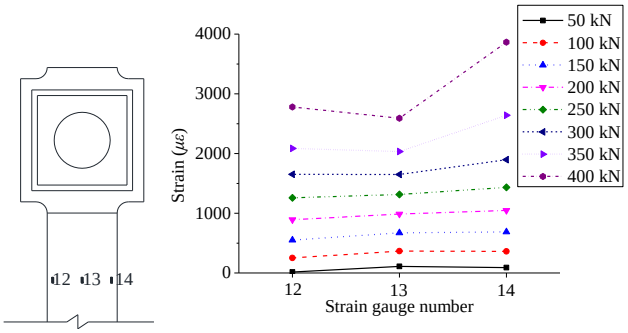

(b) Specimen SF

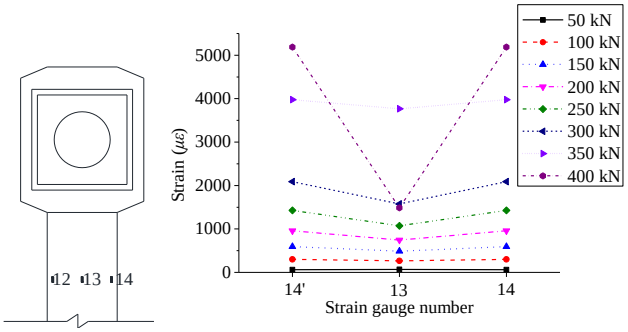

(c) Specimen ST20

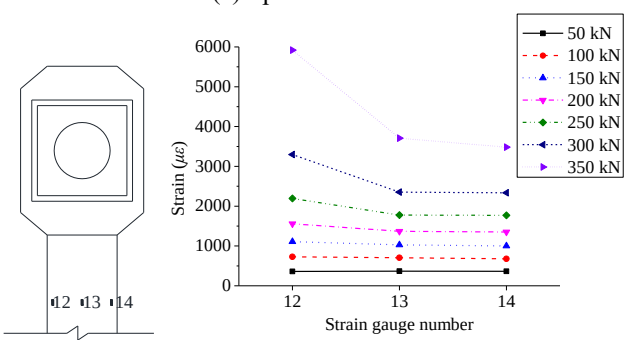

(d) Specimen ST40

Fig. 8 Strain analysis on gauges 12-14

tensile force cannot be transferred to the edges of the through-diaphragm as the strain values at points 1 and 5 are almost zero. Furthermore, the tensile force transferred to the center of the through-diaphragm is negligible.

The through-diaphragm with fillet help transfers part of the tensile force from the beam flange to the center of the through-diaphragm. It can reduce the force demand on the diaphragm. For tapered through-diaphragm, the extended length greatly affects the force flow path. The effect of the tapered through-diaphragm with relative short extended length (i.e., Specimen ST20) on the structural behavior is quite similar to that of the diaphragm with fillet. The specimen with tapered through-diaphragm of relative long extended length (i.e., Specimen ST40) has the most uniform stress distribution in the diaphragm. Significant amount of tensile force has been delivered to both the edges and the center of the through-diaphragm.

The strain distribution of the beam flange plate at the

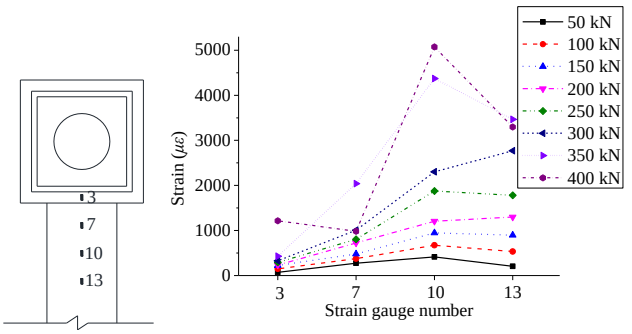

(a) Specimen SC

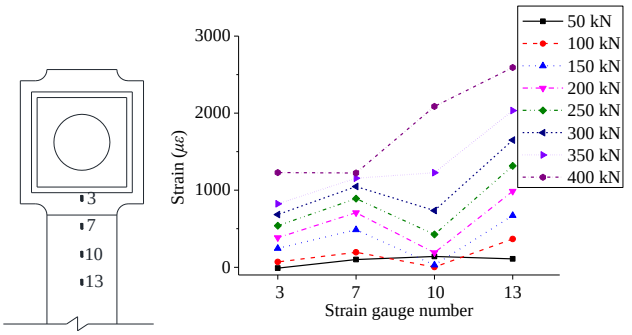

(b) Specimen SF

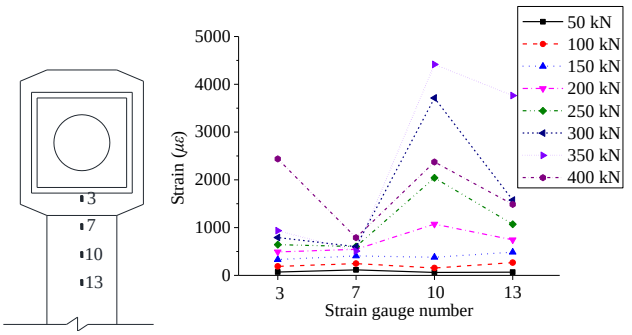

(c) Specimen ST20

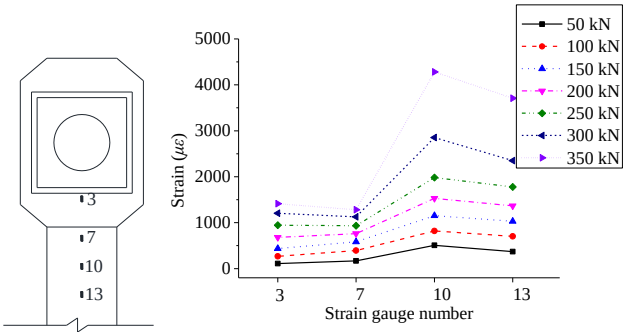

(d) Specimen ST40

Fig. 9 Strain analysis on gauges along longitudinal direction

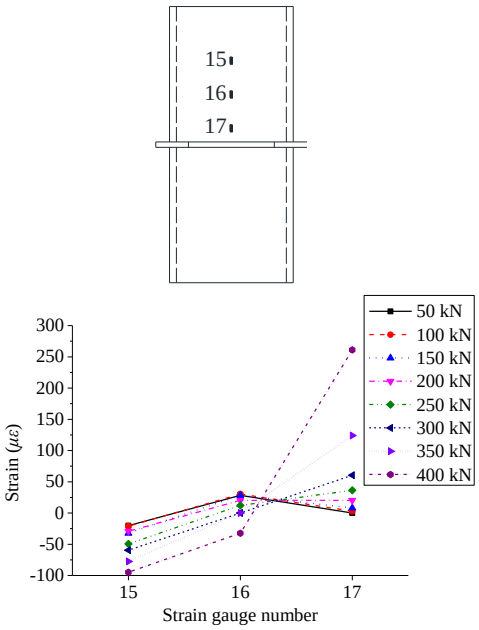

(a) Specimen ST20

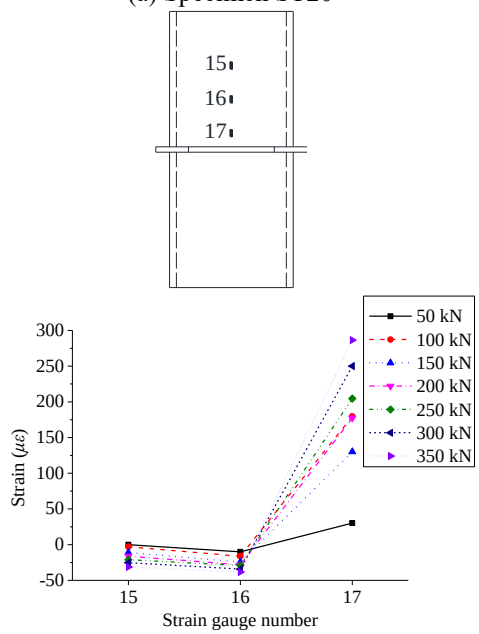

(b) Specimen ST40

Fig. 10 Strain analysis on gauges 15-17

locations 60 mm and 80 mm for Specimens SC, SF, ST20 and Specimen ST40, respectively, away from the column flange is shown in Fig. 6. For conventional through-diaphragm, the non-uniformity of stress distribution is observed at the very beginning of the load-step. More stress is concentrated at the edges of the beam flanges than at the centerline. In contrast, the connections with the improved through-diaphragm show linearly distributed stress when the loading level is low. As the tensile load continues to increase, the stress at the edges becomes larger than that at the center. Meanwhile, the comparison between Specimens ST20 and ST40 indicates that the longer extended tapered through-diaphragm exhibits more uniform stress distribution.

Fig. 7 shows the strain distribution of strain gauges 9-11. For Specimens SC, ST20, and ST40, the stress is uniformly distributed at a low level of loading. As the load increases, the stress tends to be concentrated at the center. The differences between the stress at the center and at the edges become more evident as the load continues to go up. While for Specimen SF, the trends for stress concentration is opposite.

Fig. 8 shows the stress response at a distance of 160 mm

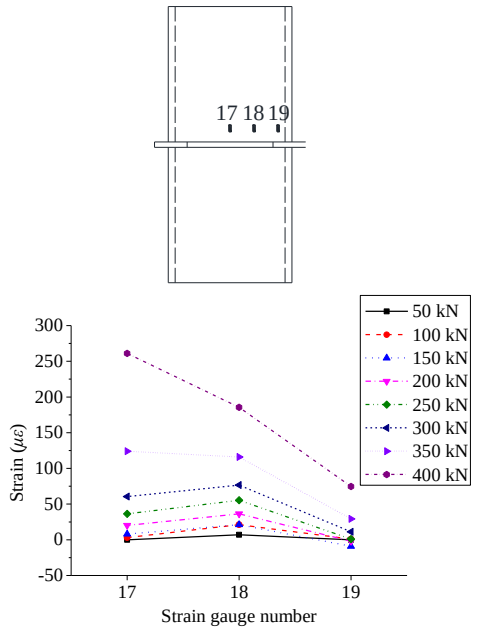

(a) Specimen ST20

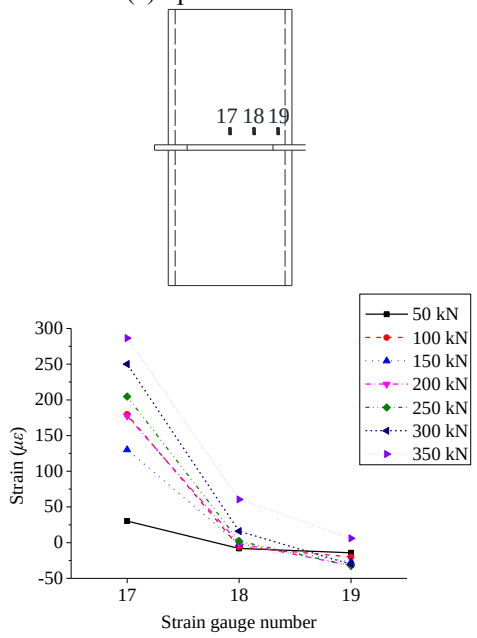

(b) Specimen ST40

Fig. 11 Strain analysis on gauges 17-19

and 180 mm away from the column flange for Specimens SC, SF, ST20 and Specimen ST40, respectively. It is obvious that the stress distribution is almost uniform until the failure of the specimens occurs. This indicates that the geometrical continuity of the specimen will not influence the location far from the connection.

The response of the strains at the center of beam flange plate along the longitudinal direction is illustrated in Fig. 9. It can be seen that the stress increases steadily with the increase in the distance from the column flange. This indirectly infers that the force flow path moves from the beam flange towards the column web. Moreover, the stress transition from the beam flange to the through-diaphragm is obviously smoother in the connections with improved through-diaphragm geometry.

The strain response of gauges 15-17 on the square tubular column is illustrated in Fig. 10. From point 17 to 15, the strain value changes from positive to negative. Meanwhile, the strain value at point 16 is close to zero. This indicates that the column flange swells out when the specimen is subjected to tensile load. Furthermore, it indirectly infers that the tensile load transferred to the column flange is finally delivered to the column web rather than along the height of the column. Meanwhile, the strain value decreases as the distance from the through-diaphragm is larger. The small strain values at points 15 and 16 show that the tensile load on the flange will not affect the deformation of the column flange at the location far from the through-diaphragm.

Fig. 11 illustrates the strain responses of gauges 17-19 on the column flange. It can be seen that the stress value gradually decreases as the distance from the center of flange gets greater. With the increase in the loading level, the stress non-uniformity becomes more obvious. Referring back to Fig. 5, it is evident that most of the strain transferred to the center of the through-diaphragm is delivered to the column flange rather than through the diaphragm. Furthermore, the strain transferred to the side of the through-diaphragm is carried directly through the diaphragm or by the column web rather than by the column flange.

4. Conclusions

Three types of improved through-diaphragm connections were proposed in this paper. Tensile tests were performed to determine the structural behavior and force flow path of the connection. The findings of this research are summarized as follows:

The load-displacement responses for all specimens are similar. The initial stiffness and the yield and ultimate loading capacity of the specimens are largely dominated by the structural behavior of the beam flange plate.

The proposed modified through-diaphragm geometries are able to reduce the stress concentration between the beam flange plate and the through-diaphragm. The stress distribution is more uniform in the specimen with tapered or fillet through-diaphragm than in the conventional through-diaphragm. Meanwhile, the extended length of the tapered through-diaphragm significantly influences the force flow path. The stress is more uniformly distributed in the specimen with longer tapered through-diaphragm.

Acknowledgments

This work is sponsored by the Natural Science Foundation of Jiangsu Province (Grant No. BK20170685), the National Key Research and Development Program of China (Grant No. 2017YFC0703802), the Prospective Joint Research Project of Jiangsu Province, China (Grant No. BY2016076-06), the state Key Laboratory of Subtropical Building Science, South China University of Technology, China (Grant No. 2018ZB26), and the Fundamental Research Funds for the Central Universities.

References

De Domenico, D., Falsone, G. and Laudani, R. (2018), "Probability-based structural response of steel beams and frames with uncertain semi-rigid connections", *Struct. Eng. Mech.*, **67**(5), 439-455.

Dehghan, S.M., Najafgholipour, M.A., Ziarati, S.M. and Mehrpour, M.R. (2018), "Experimental and numerical assessment of beam-column connection in steel moment-resisting frames with built-up double-I column", *Steel Compos. Struct.*, **26**(3), 315-328.

De Nardin, S. and El Debs, A.L.H.C. (2018), "Shear transfer mechanism in connections involving concrete filled steel columns under shear forces", *Steel Compos. Struct.*, **28**(4), 449-460.

Esfandyary, R., Razzaghi, M.S. and Eslami, A. (2015), "A parametric investigation on the hysteretic behaviour of CFT column to steel beam connections", *Struct. Eng. Mech.*, **55**(1), 205-228.

Goswami, R. and Murty, C.V.R. (2010), "Externally reinforced welded I-beam-to-box-column seismic connection", *J. Eng. Mech.*, **136**, 23-30.

Hadianfard, M.A., Hashemi, A. and Gholami, M. (2017), "Study on the effects of various mid-connections of x-brace on frame behavior", *Earthq. Struct.*, **12**(4), 449-455.

Kim, T., Stojadinovic, B. and Whittaker, A.S. (2008), "Seismic performance of pre-Northridge welded steel moment connections to built-up box columns", *J. Struct. Eng.*, **134**, 289-299.

Kim, Y.J. and Oh, S.H. (2007), Effect of the moment transfer efficiency of a beam web on deformation capacity at box column-to-H beam connections", *J. Constr. Steel Res.*, **63**, 24-36.

Kurobane, Y. (2002), "Connection in tubular structures", *Prog. Struct. Eng. Mater.*, **4**, 35-45.

Mirghaderi, S.R., Torabian, S. and Keshavarzi, F. (2010), "I-beam to boxcolumn connection by a vertical plate passing through the column", *Eng. Struct.*, **32**, 2034-2048.

Nia, Z.S., Ghassemieh, M. and Mazroi, A. (2013), "WUF-W connection performance to box column subjected to uniaxial and biaxial loading", *J. Constr. Steel Res.*, **88**, 90-108.

Nia, Z.S., Mazroi, A. and Ghassemieh, M. (2014), "Cyclic performance of flange-plate connection to box column with finger shaped plate", *J. Constr. Steel Res.*, **101**, 207-223.

Nunez, E., Torres, R. and Herrera, R. (2017), "Seismic performance of moment connections in steel moment frames with HSS columns", *Steel Compos. Struct.*, **25**(3), 271-286.

Qin, Y., Chen, Z.H. and Rong, B. (2015a), "Modeling of CFRT through-diaphragm connections with H-beams subjected to axial load", *J. Constr. Steel Res.*, **114**, 146-156.

Qin, Y., Chen, Z.H. and Rong, B. (2015b), "Component-based mechanical models for concrete-filled RHS connections with diaphragms under bending moment", *Adv. Struct. Eng.*, **18**(8), 1241-1255.

Qin, Y. and Chen, Z.H. (2016), "Research on cold-formed steel connections: A state-of-the-art review", *Steel Compos. Struct.*, **20**(1), 21-41.

Qin, Y., Chen, Z.H., Bai, J.J. and Li, Z.L. (2016), "Test of extended thick-walled through-diaphragm connection to thick-walled CFT column", *Steel Compos. Struct.*, **20**(1), 1-20.

Qin, Y., Lu, J.Y. and Cao, S. (2017), "Theoretical study on local buckling of steel plate in concrete filled tube column under axial compression", *ISIJ Int.*, **57**(9), 1645-1651.

Rezaifar, O., Nazari, M. and Gholhaki, M. (2017), "Experimental study of rigid beam-to-box column connections with types of internal/external stiffeners", *Steel Compos. Struct.*, **25**(5), 535-544.

Rong, B., You, G., Zhang, R., Ma, X. and Quan, X. (2018), "Experimental and theoretical studies on SHS column connection with external stiffening ring under static tension load", *Steel Compos. Struct.*, **28**(2), 167-177.

Shahidi, F., Rezaeian, A., Jamal-Omidi, M. and Shahidi, F. (2015), "Investigation of the ConXL moment connection cyclic behavior in box columns without filling concrete with different arrangement of collar bolts", *Struct. Des. Tall Spec. Build.*, **24**, 317-350.

Shahraki, M., Sohrabi, M.R., Aziaian, G. and Narmashiri, K. (2018), "Experimental and numerical investigation of strengthened deficient steel SHS columns under axial compressive loads", *Struct. Eng. Mech.*, **67**(2), 207-217.

Torabian, S., Mirghaderi, S.R. and Keshavarzi, F. (2012), "Moment-connection between I-beam and built-up square column by a diagonal through plate", *J. Constr. Steel Res.*, **70**, 385-401.

Wang, J., Uy, B. and Li, D.X. (2018), "Analysis of demountable steel and composite frames with semi-rigid bolted joints", *Steel Compos. Struct.*, **28**(3), 363-380.

Wang, Z.Y. and Wang, Q.Y. (2016), "Yield and ultimate strengths determination of a blind bolted endplate connection to square hollow section column", *Eng. Struct.*, **111**, 345-369.

Zhang, T., Ding, F.X., Wang, L.P. Liu, X.M. and Jiang, G.S. (2018), "Behavior of polygonal concrete-filled steel tubular stub columns under axial loading", *Steel Compos. Struct.*, **28**(5), 573-588.

Zohra, D.F. and Abd Nacer, I.T. (2018), "Dynamic analysis of steel frames with semi-rigid connections", *Struct. Eng. Mech.*, **65**(3), 327-334.

CC